

Spectropolarimetric investigation of the propagation of magnetoacoustic waves and shock formation in sunspot atmospheres

Rebecca Centeno¹, Manuel Collados¹ and Javier Trujillo Bueno^{1,2}

¹*Instituto de Astrofísica de Canarias, 38205 La Laguna, Tenerife, Spain*

²*Consejo Superior de Investigaciones Científicas (Spain)*

rce@iac.es, mcv@iac.es, jtb@iac.es

ABSTRACT

Velocity oscillations in sunspot umbrae have been measured simultaneously in two spectral lines: the photospheric Silicon I 10827 Å line and the chromospheric Helium I 10830 Å multiplet. From the full Stokes inversion of temporal series of spectropolarimetric observations we retrieved, among other parameters, the line of sight velocity temporal variations at photospheric and chromospheric heights. Chromospheric velocity oscillations show a three minute period with a clear sawtooth shape typical of propagating shock wave fronts. Photospheric velocity oscillations have basically a five minute period, although the power spectrum also shows a secondary peak in the three minute band which has proven to be predecessor for its chromospheric counterpart. The derived phase spectra yield a value of the atmospheric cut-off frequency around 4 mHz and give evidence for the upward propagation of higher frequency oscillation modes. The phase spectrum has been reproduced with a simple model of linear vertical propagation of slow magneto-acoustic waves in a stratified magnetized atmosphere that accounts for radiative losses through Newton's cooling law. The model explains the main features in the phase spectrum, and allows us to compute the theoretical time delay between the photospheric and chromospheric signals, which happens to have a strong dependence on frequency. We find a very good agreement between this and the time delay obtained directly from the cross-correlation of photospheric and chromospheric velocity maps filtered around the 6 mHz band. This allows us to infer that the 3-minute power observed at chromospheric heights comes directly from the photosphere by means of linear wave propagation, rather than from non-linear interaction of 5-minute (and/or higher frequency) modes.

Subject headings: Sun: chromosphere, Sun: oscillations, shock waves, sunspots, Sun: magnetic fields, techniques: polarimetric

1. Introduction

The study of the generation and propagation of waves in the solar atmosphere is a hot topic of research in astrophysics, since it provides information about the atmospheric structure and dynamics (e.g., Lites 1992; Bogdan 2000; Socas-Navarro, Trujillo Bueno and Ruiz Cobo, 2000; Bogdan and Judge 2006), while at the same time it helps us identify the key mechanisms of chromospheric and coronal heating. In fact, acoustic and magnetic waves and magnetic field reconnection have been mentioned in the literature as the most promising heating mechanism candidates (Alfvén 1947; Biermann 1948; Schwarzschild 1948; Parker 1979; Ulmschneider and Musielak 2003).

Historically, sunspot oscillations have been classified into three different groups (e.g. Lites 1992): (1) photospheric umbral oscillations, which have basically a 5-minute period with an average rms amplitude of 75 ms^{-1} . These oscillations are the apparent response of the umbral photosphere to the 5-minute p-mode oscillations. (2) Chromospheric umbral oscillations with periods around 180 s and amplitudes of a few kilometers per second, and (3) running penumbral waves, seen in H_α as disturbances propagating radially outwards from the umbra. They all seem to be different manifestations of the same dynamical global phenomenon, though (e.g., Rouppe van der Voort et al. 2003).

Simultaneous time-series observations of various spectral lines that sample different regions of the solar atmosphere is one of the most useful techniques for studying wave propagation (e.g., the review by Lites 1992 and references therein). For instance, Lites (1986) could provide hints of shock wave formation via the Doppler shifts observed in the Stokes I profiles of the He I 10830 Å multiplet. By measuring the phase difference of the oscillations in different spectral lines, this author could also infer the upward propagation of waves in the frequency band around 6.5 mHz (Lites, 1984). Other pioneering investigations on this topic are those by Kneer et al. (1981).

In the last 35 years, since the first report on chromospheric umbral oscillations was made (Beckers and Tallant, 1969), many works have been published on this subject, accompanied by nearly an equal number of differing findings, conclusions and contradictions yielded by the literature in this time. We refer the reader to recent reviews (such as those by Bogdan 2000 and Bogdan & Judge 2006) for a comprehensive overview of present knowledge of oscillatory phenomena in sunspots, both from the theoretical and the observational points of view.

Nowadays, theoretical investigations on this topic are mainly carried out by means of detailed numerical simulations. For instance, the hydrodynamical simulations of Carlsson & Stein (1995) suggest that acoustic shock waves in the internetwork regions of the solar atmosphere intermittently heat the plasma there, but with an acoustic shock heating that is

insufficient to explain quantitatively the emission line cores observed in far-UV lines. Similar numerical simulations have recently begun to be extended to strongly magnetized regions of the solar atmosphere, taking into account the coupling among various MHD wave modes (e.g., Stein et al. 2004), but much work remains to be done prior to reaching a level of realism for which it becomes reasonable to start contrasting computed Stokes profiles with spectropolarimetric observations. In this respect, one of the aims of this paper is to provide high-quality observational information on the phenomenon of oscillations in sunspot umbrae, based on full Stokes-vector IR spectropolarimetry in photospheric and chromospheric lines.

This paper is organized as follows: Observations, data reduction and inversion techniques are presented in sections 2 and 3. For the analysis, we follow a similar approach to that of Lites (1984, 1986) but measuring instead the full Stokes-vector of the photospheric Silicon I 10827 Å line and of the chromospheric Helium I 10830 Å multiplet. The analysis of the photospheric and chromospheric LOS velocities, and the relation between them, are shown in section 4. As we shall see below, we are able to provide very clear observational evidence for the upward propagation of waves from the photosphere to the chromosphere within the umbra of a sunspot, including an unprecedented measurement of the time delay between the signals and the detection and characterization of the photospheric driving piston. A brief discussion can be found in section 5, followed by some final remarks in section 6.

2. Observations

The observations analyzed in this paper were carried out at the German Vacuum Tower Telescope (VTT) of the Observatorio del Teide on October 1st 2000 and May 9th 2001, using the Tenerife Infrared Polarimeter (TIP, Martínez Pillet et al. 1999). This instrument allows us to take simultaneous images of the four Stokes parameters as a function of wavelength and position along the spectrograph slit, with a temporal sampling up to 0.5 seconds. In order to obtain a better signal-to-noise ratio, several images were added up on-line, with a final temporal sampling of several seconds. The slit (0".5 wide and 40" long) was placed over the targets and was kept fixed during the entire observing run (approx. 1 hour). The image stability was obtained using a correlation tracker device (Ballesteros et al, 1996) which compensates for the image motion induced by the Earth's high frequency atmospheric variability, as well as for solar rotation.

The observed spectral range spanned from 10825.5 to 10833 Å, with a spectral sampling of 31 mÅ per pixel. This spectral region is a powerful diagnostic window of the solar atmospheric properties since it contains valuable information coming from two different regions in the atmosphere (Harvey & Hall 1971; Rüedi, Solanki, Livingston 1995; Trujillo

Bueno et al. 2002; Trujillo Bueno et al. 2005; Solanki et al. 2003). It includes three spectral features. The first is a photospheric Si I line at 10827.09 Å. Next to it lies the chromospheric Helium I 10830 Å line, which is indeed a triplet, whose blue component (λ 10829.09 Å) is quite weak and difficult to see in an intensity spectrum, and whose red components (λ 10830.25, λ 10830.34 Å) appear blended. The formation mechanism of this triplet is still not fully understood, though it is thought to be generated in a thin layer in the high chromosphere, about 2000 km above the base of the photosphere (Avrett et al. 1994). The third spectral feature is a water vapour line (Rüedi et al. 1995) of telluric origin that can only be used for calibration purposes, since it generates no polarization signal.

We chose two different target sunspots for the analysis presented in this paper. On both occasions the slit was placed over the center of the sunspot. Table 1 shows the details for both data sets.

3. Data reduction and inversion

Flatfield and dark current measurements were performed at the beginning and the end of both observing runs and, in order to compensate for the telescope instrumental polarization, we also took a series of polarimetric calibration images. The calibration optics (Collados 1999) allows us to obtain the Mueller matrix of the light path between the instrumental calibration sub-system and the detector. This process leaves a section of the telescope without being calibrated, so further corrections of the residual cross-talk among Stokes parameters were done: the I to Q, U and V cross-talk was removed by forcing to zero the continuum polarization, and the circular and linear polarization mutual cross-talk was calculated by means of statistical techniques (Collados 2003).

In order to infer the physical parameters of the magnetized atmosphere in which the measured spectral lines were generated, we carried out the full Stokes inversion of both the Silicon line and the Helium triplet within the umbra of the sunspot for the whole time series of observations and for both data sets. Thus, we were able to obtain the temporal variability of several physical quantities (line of sight velocity, magnetic field intensity and orientation...) at the photospheric and chromospheric regions where the observed spectral line radiation originates, though in this paper we will concentrate only on the results concerning the line of sight velocity temporal fluctuations. We could have used a simpler method to infer Doppler velocities rather than inversion techniques, but we decided to stick to the latter after comparing the results with those obtained from a preliminary analysis (in which we calculated velocities by measuring directly the position of the intensity minimum and the Stokes V zero-crossing), and finding that they yielded very similar results.

The information encoded in the Silicon line radiation was retrieved by using the code LILIA, developed by Socas-Navarro (2001). LILIA is a package for the synthesis and inversion of Stokes profiles induced by the Zeeman effect. It is based on the assumption of local thermodynamic equilibrium (LTE), and takes into account the Zeeman induced polarization pattern of the spectral lines. A guess atmosphere is iteratively modified by the code, using a Levenberg-Marquardt minimization algorithm (Press et al. 1988), until the synthetic profiles mimic the observed ones, in a least square sense. LILIA returns not only the values for the thermodynamic and physical parameters, but also their stratification in the atmosphere. All the values for photospheric parameters presented from now on in this paper, refer to the height corresponding to $\log(\tau_{500}) = -2$.

The inversion of the Helium lines was carried out using a code based on the Milne-Eddington (ME) approximation, similar to that described by Socas-Navarro, Trujillo Bueno & Landi Degl’Innocenti (2004). We decided to give no weight to the blue component of the triplet in the inversion because it seemed to be contaminated with some other unknown spectral feature, whose possible physical origin is discussed in Centeno et al. (2005). Although the ME approach does not provide the stratification of the atmospheric parameters, it returns precise velocity values and an average (over the region of formation) for the rest of the magnitudes (see, e.g., Westendorp Plaza et al. 1997).

4. Analysis

4.1. Shock waves

Figure 1 shows the temporal evolution of the Stokes V profiles for one position inside the umbra of sunspot #1 obtained directly from the observations. The horizontal and vertical axes represent time and wavelength, respectively (the origin of wavelength scale being the rest position of the Silicon line). Around the zero-wavelength position we see the Silicon Stokes V profile, which at first sight does not seem to change with time. On the other hand, the upper part of the figure shows the evolution of the circular polarization observed in the Helium multiplet, with the high contrasted red components on top (at $\sim 3.3 \text{ \AA}$) and the blue component rather weak, underneath (at $\sim 2 \text{ \AA}$). Both signals exhibit the same behaviour: the positions of the zero-crossing of the Stokes profiles show periodic shifts in wavelength with a clear sawtooth shape (i.e. sudden blue-shifts followed by slower red-shifts), suggestive of shock wave trains.

It is interesting to note that the Stokes V profiles show irregular shapes during blue-shifts, suggesting they are not resolved within the temporal and/or spatial sampling of our observa-

tions or even that they are simply the result of integration along the line-of-sight in a shocked plasma. This happens not only for sunspot #1 (with a 7.9s sampling) but also for sunspot #2 (with a much finer sampling of 2.1s). Figure 2 shows two different Stokes V profiles for the Helium triplet, corresponding to a unique position inside the umbra of sunspot #1. The two profiles were measured at different times: while the one on top corresponds to a snapshot of a redshift, the one on the bottom was measured while the Helium line was undergoing a blueshift.

4.2. Results from the inversions

After carrying out the full Stokes inversion of the Silicon line and the Helium triplet inside the umbrae of sunspots #1 and #2, we obtained the temporal variation of the atmospheric structure at the photosphere and the chromosphere, for all the positions along the slit. We will focus on the results for the line of sight velocity in this paper. As mentioned earlier, the analysis of the remaining retrieved parameters will be left for a subsequent paper.

Figure 3 shows the photospheric (above) and chromospheric (below) line of sight velocity maps for the umbra of sunspot #2, obtained from the inversions of the Silicon and Helium lines respectively. The horizontal and vertical axes represent time and position along the slit. Black means negative velocity (matter approaching the observer). In both maps, we have subtracted a slow linear variation of the velocity due to the Sun-Earth relative motion. The phase of the oscillations changes slowly across the umbra in the chromosphere, while in the photosphere this variation is even slower, and the oscillations seem to keep the coherence over larger regions. The typical size of a photospheric patch is 5 to 10 arcsec while the size of a chromospheric patch is between 2 and 5 arcsec.

Figure 4 shows the temporal evolution of the photospheric (left) and chromospheric (middle) line of sight velocities for one position inside the umbra of sunspot #2. The photospheric velocity, with an rms noise level of about 30 ms^{-1} , shows an approximately sinusoidal pattern with a peak to peak amplitude of 400 ms^{-1} and a period within the five minute band. On the other hand, chromospheric velocity oscillations (shown in more detail in the right panel of Figure 4) have a well defined three minute period and quite large peak to peak variations (of the order of $10\text{-}15 \text{ kms}^{-1}$). Also, the oscillation pattern has a clear sawtooth shape that indicates the presence of shock wave trains at chromospheric heights, as already mentioned in the former section.

4.3. Power spectra.

Figure 5 shows the power spectra averaged over the entire umbra of sunspot #1 (top) and sunspot #2 (bottom), for both the chromospheric (solid) and the photospheric (dashed) velocity signals. In the chromospheric signal, power is concentrated between 5 and 8 mHz (3 minute band) with a clear peak around 6 mHz. Note that there is nearly no power at all in the 5 minute band (~ 3.3 mHz). On the other hand, the photospheric velocity power spectrum has most of its power concentrated in the range from 2 to 5 mHz, which corresponds to the well known five minute oscillations. But there are also secondary peaks between 5 - 7 mHz which we believe to be the photospheric counterpart of the chromospheric 3-minute oscillations, as will be shown further on.

4.4. Phase diagrams

The upper part of Figure 6 shows the phase difference ($\Delta\phi$) between the chromospheric and the photospheric velocity signals, as a function of frequency. On the left, the results for umbra #1, and on the right for umbra #2. Each cross on the figure is obtained as the difference from the chromospheric phase and the photospheric phase for one frequency and one position inside the umbra of the sunspot. The phases are obtained directly from the Fourier transform of the velocity signals, for each position along the slit. Note that there is a 2π indetermination in the computation of the phase value, so the phase difference will be cyclic every 2π .

The lower part of Figure 6 shows the coherence spectra for both data sets. Coherence spectrum is intimately related to phase spectrum and it tells us whether the phase difference between two signals for one harmonic ω is characteristic of the signals or, on the contrary, is an arbitrary feature. For this reason, coherence is a statistical definition, and makes no sense when calculated between two velocity signals measured at two different heights and the same spatial position. The horizontal line delimits the confidence limit at 0.7, above which we consider the coherence is significant, and the information given by the phase spectrum is reliable (between 2.5 - 7 mHz for sunspot #1, and between 3 - 8.5 mHz for sunspot #2).

From Figure 6 we can see that in the range from 0 to 2 mHz, the phase spectrum is very noisy (in both cases), with a mean value around zero, indicating that the oscillation modes at photospheric heights have nothing to do with the same modes observed at chromospheric heights, i.e. there is no wave propagation in this frequency regime. From 2 up to, approximately, 4 mHz, the phase spectrum is not so noisy but values still remain very near zero, indicating that there is no propagation, but what we see are standing waves (i.e., waves that

are reflected somewhere below the level of formation of the Si line). From 4 mHz on, the phase spectrum shows a clear increasing tendency meaning that these frequency modes do propagate from the photosphere reaching the chromosphere at some point.

4.4.1. The theory

Just for a reason of completeness and self-containment, in this subsection we make a brief overview of some basic models for wave propagation in plane-parallel atmospheres, following works available in the literature (Ferraro and Plumpton 1958, Souffrin 1972, Mihalas and Mihalas 1984, Bünte and Bogdan 1992). Beginning with an adiabatic stratified atmosphere, we will compare it to a non-stratified one, and after that, to an atmosphere that allows for radiative losses through Newton’s cooling law. We will see that this last case agrees reasonably well with the observations.

Consider a standard plane-parallel isothermal stratified atmosphere permeated by a uniform vertical magnetic field (as in Ferraro and Plumpton, 1958). If we introduce a small adiabatic perturbation with a frequency ω , and study its propagation, in the linear regime these authors find two independent solutions: an Alfvén wave (transversal in nature, propagating along the field lines) and a sound wave (also propagating along the field lines, but longitudinal and totally unaware of the presence of the magnetic field). As we are studying the propagation of longitudinal velocity oscillations along the magnetic field lines, we are only interested in the sound wave. The amplitude $A(z)$ of the generated monochromatic wave appears as the solution to the differential equation

$$c^2 \frac{d^2 A(z)}{dz^2} - \gamma g \frac{dA(z)}{dz} + \omega^2 A(z) = 0, \quad (1)$$

where z is the cartesian vertical coordinate, H_0 is the pressure scale height, g is the gravity (assumed constant), $c^2 = \gamma g H_0$ the speed of sound and $\gamma = c_p/c_v$ the ratio of specific heats, which in the case of an adiabatic propagation is strictly equal to 5/3 for a monoatomic plasma. If we introduce the solution $A(z) = e^{ik_z z}$ (where k_z represents the vertical wavenumber) in Eq. (1), we end up with a dispersion relation of the form:

$$k_z = \frac{1}{c} (-i\omega_{ac} \pm \sqrt{\omega^2 - \omega_{ac}^2}), \quad (2)$$

where

$$\omega_{ac} = \gamma g / 2c \quad (3)$$

is the cut-off frequency. When k_z takes an imaginary value ($\omega < \omega_{ac}$), the solution $A(z)$ is damped and there is no wave propagation. On the contrary, when k_z has a real part ($\omega > \omega_{ac}$), the solution is a purely upward (downward) propagating wave that increases (decreases) its amplitude as it reaches higher (lower) levels of the atmosphere. This behavior can be inferred from the equations

$$(\omega < \omega_{ac}) \quad A(z) = e^{\frac{\omega_{ac} \pm \sqrt{\omega_{ac}^2 - \omega^2}}{c} z} \quad (4)$$

$$(\omega > \omega_{ac}) \quad A(z) = e^{z\omega_{ac}/c} e^{\frac{\pm i \sqrt{\omega^2 - \omega_{ac}^2}}{c} z} \quad (5)$$

Below the cut-off frequency, oscillations do not propagate, being instead evanescent in character, and generating standing waves. In the case of standing waves, the difference in phase of the oscillations measured at whatever heights are chosen, is always zero. Above the cut-off value, oscillation modes propagate with a phase velocity that depends on the frequency. The phase of the oscillation is the argument of the complex exponential ($\phi = c^{-1} \sqrt{\omega^2 - \omega_{ac}^2} z$), and the phase difference of the oscillations of a propagating wave measured at two heights will be $\Delta\phi = c^{-1} \sqrt{\omega^2 - \omega_{ac}^2} \Delta z$, where Δz is the geometric distance between the two levels.

The dot-dashed line in Figure 7 represents the phase difference of the oscillations measured at two fixed heights for the case of linear adiabatic vertical propagation in an isothermal stratified atmosphere. Below the cut-off frequency (~ 3.7 mHz in this simulation) nothing propagates, while above it, modes start to propagate with a phase speed that decreases with frequency. The medium is then dispersive. The dashed line (just for comparison) shows the case for linear adiabatic wave propagation in an isothermal non-stratified atmosphere (without gravity). In this case, the phase difference is linear with frequency, meaning that the phase velocity is the same for all the oscillation modes, and that there exists no cut-off frequency - i.e. all modes propagate. This is the case of a non-dispersive medium.

If, instead of an adiabatic propagation, we relax this condition allowing for radiative losses with a simple Newton's cooling law (following Mihalas and Mihalas 1984, but originally developed by Souffrin, 1972), the picture we obtain is somewhat different. Newton's cooling law accounts for the damping of the temperature fluctuations due to radiative losses, with a typical cooling time τ_R given by:

$$\tau_R = \rho c_v / (16\chi\sigma_R T^3), \quad (6)$$

where χ is the mean absorption coefficient and σ_R is the Stefan-Boltzmann constant. We can use their solution for vertical propagation of longitudinal waves (i.e. zero horizontal wavenumber $k_x = 0$) in the case of the propagation of acoustic-gravity waves in a radiating fluid for a non-magnetic isothermal atmosphere. The reason that allows us to do this, is based on the fact that sound waves propagating along vertical magnetic field lines are unaware of the presence of the magnetic field. This means that the differential equation for sound waves propagating along a vertical magnetic field will be formally identical to the one for the field free case. The solution inserted into the differential equation

$$A(z) = D e^{z/(2H_0)} e^{ik_z z} \quad (7)$$

yields to the following dispersion relation:

$$k_z^2 = \frac{\omega^2 - \hat{\omega}_{ac}^2}{\hat{c}^2}, \quad (8)$$

where, following the definitions by Bunte and Bogdan (1992)

$$\hat{\omega}_{ac} = \hat{c}^2/4H_0; \quad \hat{c}^2 = \hat{\gamma}gH_0; \quad \hat{\gamma} = \frac{1 - \gamma i\omega\tau_R}{1 - i\omega\tau_R}. \quad (9)$$

We can compute the real and the imaginary parts of k_z :

$$k_R^2 = \frac{1}{2}[h_R + (h_R^2 + h_I^2)^{1/2}], \quad (10)$$

$$k_I^2 = \frac{1}{2}[-h_R + (h_R^2 + h_I^2)^{1/2}], \quad (11)$$

where

$$h_R = \frac{\omega^2(1 + \omega^2\tau_R^2\gamma)}{gH_0(1 + \omega^2\tau_R^2\gamma^2)} - \frac{1}{4H_0^2} \quad (12)$$

$$h_I = \frac{(\gamma - 1)\tau_R\omega^3}{(1 + \omega^2\tau_R^2\gamma^2)gH_0}. \quad (13)$$

Both k_R and k_I are real, and the curves $h_R = 0$ define the boundaries between mainly propagating ($k_R > k_I$) and mainly damped ($k_R < k_I$) waves. The solid line in Figure 7

shows us what the phase spectrum would look like in this case. Now, there is no cut-off frequency as such, being all modes propagated and reflected at the same time, with a ratio of propagation versus reflection increasing as a function of frequency. The transition between propagating and non-propagating regimes is not so clear though a pseudo-cut-off frequency can be defined. When the typical radiative time scale τ_R is small enough (of the order of tens of seconds), this effective cut-off frequency turns out to be much smaller than the one obtained for the adiabatic case.

4.4.2. *Combining theory and observations*

We were able to fit the phase spectra with this last assumption (stratified atmosphere allowing for radiative losses) which leaves three free parameters: the temperature of the model atmosphere T , the difference in heights Δz at which the oscillations are measured, and the typical time scale in which the temperature fluctuations are damped radiatively, τ_R .

The model accounts for the effective cut-off frequency, the slow transition between the propagating and non-propagating regimes, and the slope of the phase spectra above the atmospheric cut-off. The solid line in Figure 6 shows the best fit for both data sets. The values used for the fits are detailed in Table 2 and will be discussed in section 5. The model accounts not only for the phase spectra, but also for the amplification factor of the chromospheric signals relative to their photospheric counterpart, as a function of frequency. Figure 8 shows the ratio of chromospheric over photospheric power as a function of frequency for both data sets. Overplotted to the observational ratio, we show the theoretical one (in dashed line) obtained from the best-fit-parameters applied to the model. Below 3 mHz the data are not reliable due to the S/N ratio, but note that above this value, the agreement is quite good (in tendency and order of magnitude). Authors before have tried to fit phase spectra with the non-stratified model, which cannot even reproduce a cut-off frequency, not to talk about the change in slope of the phase spectrum. Taking into account that the atmospheric model we use is very simple (isothermal and linear), the fits agree reasonably well with the observations and account for the main features.

4.5. Filtering

In order to determine how the photospheric power spectrum 3-minute peak is related to the chromospheric oscillation, we filter the velocity signals in narrow bands around 6 mHz (where power is significant at both heights) for each point inside the slit. This allows us to

compare the photospheric and chromospheric filtered velocity maps and see what time shift we have to apply between them so that they match each other.

From the curve that fits the phase spectrum, we can easily obtain the group velocity ($v_g = d\omega/dk$), and from that, the time that it would take for each oscillating mode to reach the chromosphere from the photosphere ($t_{delay} = \Delta z/v_g$).

Figure 9 shows the time (solid line) that a quasi-monochromatic photospheric perturbation would take to reach the chromosphere, calculated directly from the fit to the phase spectra of both data sets. The phase velocity, and consequently the time delay, is highly dependent on frequency. This implies that, in order to estimate the time that a perturbation originated in the low photosphere takes to reach the high chromosphere, we should compare the modulation pattern of the velocity signals filtered in narrow frequency bands, so that the propagating time does not vary significantly within the filtering range.

We take both the photospheric and the chromospheric line of sight velocity maps and we filter them in three narrow frequency bands: 4 - 5, 5 - 6 and 6 - 7 mHz. We are not interested in the signals below 4 mHz since from the phase spectrum we see that there is no significant wave propagation in this range. Above 7 mHz, the phase spectrum becomes very noisy, and the signal in the power spectrum too low to be trusted. After comparing each pair of maps filtered in the same frequency range, we find that the external photospheric and chromospheric modulation patterns resemble each other, but, in order to make them match, a temporal shift has to be applied between them.

Figure 10 shows the filtered chromospheric (solid) and photospheric (dashed) velocity signals in the 4 - 5 mHz range, for two positions (upper and lower panels) inside umbra #2. We have shifted the photospheric velocity signal with respect to the chromospheric one in order to achieve a correspondence between the modulation patterns, yielding a time delay of roughly 40 seconds. The sense of the shift is such that what happens in the photosphere comes before the corresponding chromospheric events - i.e. upward propagation. Figures 11 and 12 are completely analogous to Figure 10, but filtered in the 5 - 6 and 6 - 7 mHz bands respectively. The time delay we had to apply was 242 s in the first case, and 248 s in the second one.

Stars overplotted to the theoretical time delay in Fig. 9 correspond to the temporal shift we had to apply between photospheric and chromospheric filtered velocity maps in order to make them match. Even though the theoretical curve predicts a strong variation of the time delay within the 1 mHz filtering bands, the agreement between theory and observations is pretty good.

The measured time delay remains constant along the slit within each filtering frequency

band. We find that the match in the shape of the modulation schemes of the photospheric and chromospheric signals is not just a coincidence, but remains along most of the umbra (for both sunspots analyzed in this paper). Only the edges of the umbra show mismatch between the signals. This is a consequence of the magnetic field lines opening up as they approach higher layers in the solar atmosphere. Wave propagation is taking place along these field lines, implying that the modulation pattern of the oscillation broadens as the waves propagate higher in the atmosphere, so we will not see the edges of the photospheric map in the chromospheric one.

5. Discussion

Many authors before us have given evidence for the upward propagation of waves in the solar atmosphere. For instance, Brynildsen et al. (2003, 2004) talk about propagation from the upper chromosphere to the transition region and into the corona, based on spectroscopic observations made with TRACE and SUMER of transition region lines. They find that the 3 min oscillations are easier to measure in the blue wings of these lines than in the red wings, giving support to the hypothesis of upwardly propagating acoustic disturbances.

In this paper, we study the relationship of the line of sight (LOS) velocity signals at the low photosphere and the high chromosphere inside umbral atmospheres by means of spectropolarimetry in the near-IR spectral region around 10830 Å. Photospheric power spectra show a non-negligible amount of power in the 6 mHz band (3 min oscillations) within the umbrae of both sunspots. Analyzing the LOS velocity phase spectra for both data sets, we find that the power above 4 mHz indeed reaches the chromosphere, while for lower frequencies the energy does not seem to propagate up to those heights. We managed to fit the phase and amplification spectra with a simple model of linearized vertical wave propagation in a stratified atmosphere which allows for radiative losses. The model accounts for the effective cut-off frequency, the slow transition between the propagating and non-propagating regimes, the slope of the phase spectra above the ω_{ac} and the amplification factor of chromospheric versus photospheric power as a function of frequency. Taking into account the simplicity of the model (which depends only on three free parameters), we cannot expect very realistic numbers for the physical magnitudes yielded from the fits. But, interestingly, the retrieved values seem to be somewhat coherent with what one would expect. The height difference between the layers of formation of the Silicon and de Helium lines is the same for both sunspots. On the other hand, the temperature is lower inside the biggest sunspot, in agreement with Collados et al. (1994) and Maltby (1992). Another issue is the value obtained for the typical radiative relaxation time, which is smaller for the largest

sunspot (#1). If we assume a monolithic model for sunspot umbrae, we would expect larger values of τ_R the more homogeneous the structure. Smaller values of τ_R should be related to larger temperature inhomogeneities, what, at first sight, is incompatible with our results. However, this disagreement could be explained if we take into account that sunspot #1, although larger, was actually divided by a faint light bridge, being more inhomogeneous in nature than sunspot #2.

The model also gives us the time delay we should expect between photospheric and chromospheric signals, which happens to be extremely dependent on the frequency of the propagating mode. In order to compare this with the data, we filtered the velocity maps in three narrow frequency bands: 4 - 5, 5 - 6 and 6 - 7 mHz. Then we compared each pair of photospheric and chromospheric maps filtered in the same frequency range, finding that the external modulation patterns resemble each other. This shows clearly the temporal shift we have to apply to one of the maps in order to make it match the other one. This method yields to values for the time delay that agree reasonably well with the prediction by the theoretical model.

All along this paper we have assumed linear propagation of waves disregarding the effects of non-linear terms in the MHD equations, although in our data sets there is clear evidence for non-linearity of the velocity oscillations at chromospheric heights (i.e. shock waves). Is the linear approximation still valid in this case?

Many authors before (see e.g. Fleck and Schmitz 1993) have argued about the possibility of non-linear interaction among the 5-minute (or even high frequency) modes being the source of the three minute oscillations. The non-linear terms in the MHD equations would take some power from the 5-minute band and convert it into higher frequency modes, thus giving rise to the 3-minute oscillations. If, in between the Silicon and the Helium levels of formation this were the case, the five-minute band would be contributing to the generation of the three minute power along all the distance in between photosphere and the high chromosphere, and so the chromospheric signal would not resemble the photospheric one at all at the same frequency. This does not agree with the fact that there exists a clear correlation between photospheric and chromospheric velocity maps in the 6 mHz frequency range. We can conclude that, in between the levels of formation of the Silicon and the Helium lines, the non-linear interaction among the 5-minute modes is not the main cause of the 3-minute power. Of course there can still be some of this taking place, but the main contribution to the chromospheric oscillations comes directly from the photosphere.

On the other hand, the saw-tooth shape of the chromospheric velocity signals is related to high frequency terms in the chromospheric power spectrum. These high frequency modes appear probably as a consequence of non-linear interaction among 3-minute modes, since

the amplitude of chromospheric oscillations is such that the linear assumption cannot be made anymore. Our study is restricted to the region of the spectra below 8 mHz, so we are ignoring these high frequency modes, and with them, the effects of non-linearity.

A different but related issue is the final origin of the 3-minute power at photospheric heights, which may come from non-linear processes or have a completely independent cause. The information we get from our data cannot address this still open question. It seems clear to us that the oscillation pattern measured in the chromosphere can clearly be seen at photospheric layers. Wherever (or whatever) the source is, at some point, the 3-minute mode gets to the photosphere and several minutes later reaches the high chromosphere.

6. Conclusions

The spectropolarimetric investigation we have presented here provides observational evidence for the upward propagation of slow magneto-acoustic waves from the photosphere to the high chromosphere inside the umbra of a sunspot. The time delay between the signals corresponding to both regions varies strongly with the frequency of the oscillation, going from a few tens of seconds to several minutes. As the photospheric perturbations propagate upwards, their amplitude increases due to the rapid decrease in density, and they eventually develop into shock waves at chromospheric heights.

Interestingly, the observed temporal variability of the Stokes profiles in the Si I line at 10827.09 Å may help to establish the required initial condition for performing realistic MHD simulations, which are needed for a full physical understanding of the phenomenon of wave propagation in sunspot atmospheres. Our future work on this topic will focus on similar spectropolarimetric investigations, but for atmospheric plasma structures with lower magnetic fluxes, such as pores, active region plages and the chromospheric network of the ‘quiet’ Sun.

It is a pleasure to thank Héctor Socas-Navarro and José Antonio Bonet for fruitful discussions and for sharing with us their knowledge on Stokes inversion techniques and Fourier analysis. We are also grateful to Bruce Lites and Tom Bogdan for suggesting improvements to an earlier version of this paper. This research has been funded by the Spanish Ministerio de Educación y Ciencia through the project AYA2004-05792, and is part of the European Solar Magnetism Network.

REFERENCES

- Alfvén, H. 1947, MNRAS, **107**, 211.
- Avrett, E.H., Fontenla, J.M., Loeser, R., 1994, in *Infrared Solar Physics*, International Astronomical Union Symposium **154**, (eds.) D.M. Rabin, J. Jefferies and C.A. Lindsay, 35-47.
- Ballesteros, E., Collados, M., Bonet, J.A., Lorenzo, F., Viera, T., Reyes, M., Rodríguez Hidalgo, I., 1996, *Astron. Astrophys.* **115**, 353.
- Beckers, J.M., Tallant, P.E., 1969, *Solar Physics* **7**, 351.
- Biermann, L. 1948, *Z. Astrophys.*, **25**, 161.
- Bogdan, T.J., 2000, *Solar Physics* **192**, 373-394.
- Bogdan, T.J., Judge, P.G., 2006, *Phil. Trans. Roy. Soc. Lond.* (in press).
- Brynildsen, N., Maltby, P., Fredvik, T., Kjeldseth-Moe, O., ESA SP-547, January 2004.
- Brynildsen, N., Maltby, P., Kjeldseth-Moe, O., 2003, *A&A* **398**, 15-18.
- Büntje, M., Bogdan, T.J., 1994, *A&A*, **283** 642.
- Carlsson, M., Stein, R.F., 1995, *ApJ*, **440**, L29.
- Centeno, R., Socas-Navarro, H., Collados, M., Trujillo Bueno, J. 2005, *ApJ*, in press.
- Collados, M., 1999, in “Third Advances in Solar Physics Euroconference: Magnetic fields and Oscillations”, edited by B. Schmieder, A. Hofmann and J. Staude, ASP Conference Series, vol. **184**, pp. 3-22.
- Collados, M., 2003, in “Polarimetry in Astronomy”, edited by Silvano Fineschi, Proceedings of the SPIE, vol. **4843**, pp. 55-65.
- Collados, M., Martínez Pillet, V., Ruiz Cobo, B., del Toro Iniesta, J.C., Vázquez, M., 1994, *A&A*, **291**, 622.
- Ferraro, V.C.A., Plumpton, C., 1958, *Apj*, **127**, 459.
- Fleck, B., Schmitz, F. 1993, *A&A*, **273**, 671.
- Harvey, J., Hall, D., 1971, *IAUS* **43**, 279.

- Kneer, F., Mattig, W., Uexkuell, M.V., 1981, *A&A* **102**, 147.
- Lites, B. W., 1984, *ApJ*, **277**, 874.
- Lites, B. W., 1986, *ApJ*, **301**, 1005.
- Lites, B. W., in “Sunspots: Theory and Observations” edited by J. H. Thomas and N. O. Weiss, 1992, pp. 261-302.
- Maltby, P., 1992, in Sunspots: Theory and Observations, J.H. Thomas and N.O. Weiss (Eds.), Kluwer, 103.
- Martínez Pillet, V., Collados, M., Sánchez Almeida, J. et al., 1999, in *High Resolution Solar Physics: Theory, Observations and Techniques*, ASP Conference Series **183**, (eds.) T.R. Rimmele, K.S. Balasubramaniam, and R. Radick, 264.
- Mihalas, D., Mihalas, B.W., 1984, “Foundations of Radiation Hydrodynamics”, Oxford University Press.
- Parker, E.N., 1979, “Cosmical Magnetic fields”, Clarendon Press. Oxford.
- Press, W.H., Flannery, B.P., Teukolsky, S.A., Vetterling, W.T., 1988, “Numerical Recipes in C”, Cambridge University Press.
- Roupe van der Voort, L.H.M., Rutten, R.J., Sütterlin, P., Sloover, P.J., Krijger, J.M., 2003, *A&A*, **403**, 277.
- Rüedi, I., Solanki, S.K., Livingston, W.C., 1995, *A&A* **293**, 252.
- Schwarzschild, M. 1948, *H.*, *ApJ*, **107**, 1.
- Socas-Navarro, H., 2001, in “Advanced Solar Polarimetry – Theory, Observation, and Instrumentation”, edited by M. Sigwarth , **236**, p. 487.
- Socas-Navarro, H., Trujillo Bueno, J., Landi Degl’Innocenti, E., 2004, *ApJ* **612**, 1175.
- Socas-Navarro, H., Trujillo Bueno, J., Ruiz Cobo, B., 2000, *Science* **288**, 1396.
- Souffrin, P., 1972, *A&A*, **17**, 458.
- Solanki, S.K., Lagg, A., Woch, J., Krupp, N., Collados, M., 2003, *Nature* **425**, 692.
- Stein, R.F. et al., 2004, Proc. of SOHO 13 “Waves, Oscillations and Small-Scale Transient Events in the Solar Atmosphere: a Joint View from SOHO and TRACE”, Palma de Mallorca, Balearic Islands (Spain), 29 September - 3 October 2003 (ESA SP-547, January 2004).

Trujillo Bueno, J., Merenda, L., Centeno, R., Collados, M., Landi Degl’Innocenti, E., 2005, *ApJ*, **619**, 191.

Trujillo Bueno, J., Landi Degl’Innocenti, E., Collados, M., Merenda, L., Manso Sainz, R., 2002, *Nature* **415** 403.

Ulmschneider, P., Musielak, Z., 2003 in “Current Theoretical Models and Future High Resolution Solar Observations: Preparing for ATST”, *ASP Conference Series*, **286**, 363.

Westendorp Plaza, C., del Toro Iniesta, J.C., Ruiz Cobo, B., Martínez Pillet, V., Lites, B.W., Skumanich, A., 1997, 1st *Advances in Solar Physics Euroconference*, *Advances in the Physics of Sunspots*, *ASP Conference Series* **118**, 197-201.

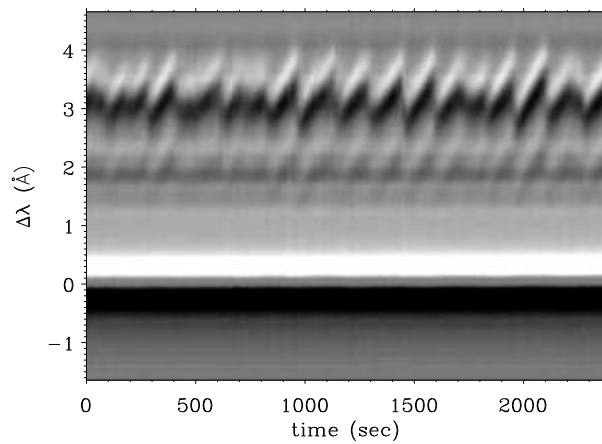


Fig. 1.— Temporal evolution of Stokes V. The horizontal axis represents time, increasing to the right, and the vertical axis wavelength (with origin at the position of the Silicon rest wavelength). The Silicon Stokes V profile (lower part of the figure) shows no apparent change with time in this presentation, while Helium profiles (upper part) show periodic Doppler shifts with a clear saw-tooth shape.

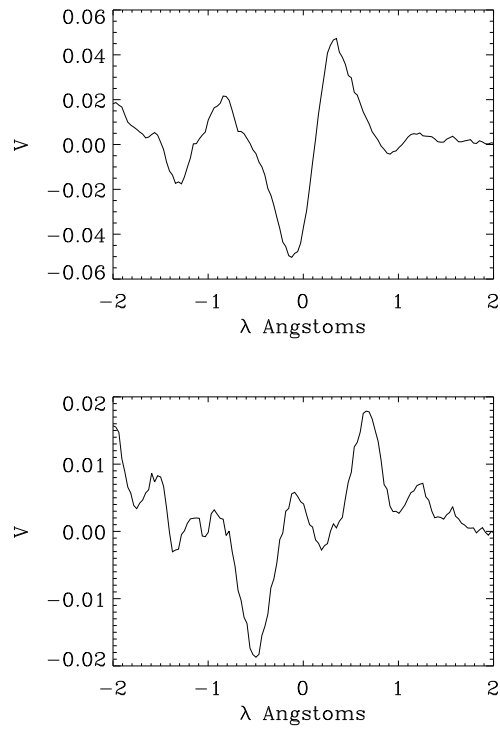


Fig. 2.— **Top:** Normal Stokes V profile while the line is undergoing a redshift. **Bottom:** Complex shaped Stokes V profile while the line is undergoing a blueshift.

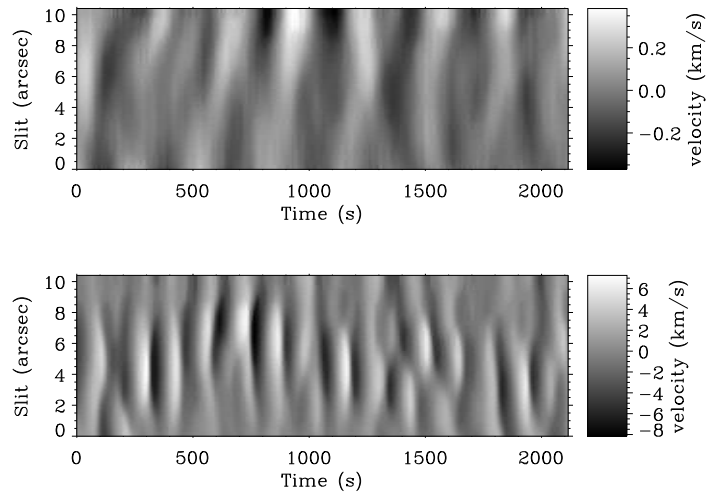


Fig. 3.— Velocity maps for the photosphere (above) and the chromosphere (below) inside the umbra of sunspot # 2. Horizontal axis represents the time (in seconds) and vertical axis the position along the slit (arcsecs). Black means negative velocity (material approaching the observer).

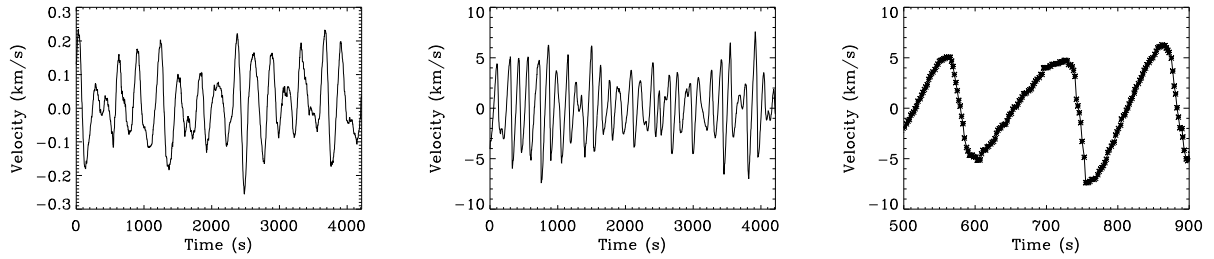


Fig. 4.— Photospheric (**left**) and chromospheric (**middle**) line of sight velocity signals as a function of time, for one point of the slit inside the umbra of sunspot #2. **Right**: Detail of chromospheric velocity at one point of the slit. The stars represent the measured values. The sawtooth shape is clearly seen, with a slow evolution of the velocity towards positive values followed by a sudden blue-shift, indicating the presence of shock waves

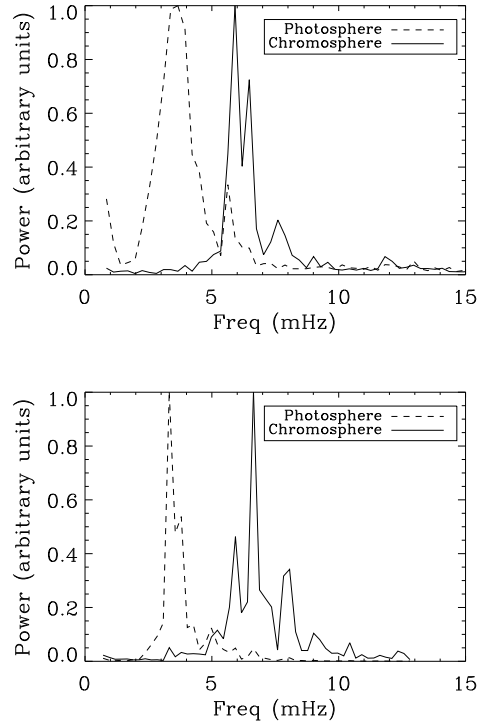


Fig. 5.— Average umbral power spectra for sunspot #1 (top) and for sunspot #2 (bottom). **Solid:** Power spectrum of the chromospheric velocity oscillations averaged over the umbra, with a peak around 6 mHz. **Dashed:** Photospheric velocity power spectrum averaged over the entire umbra, with a peak around 3.3 mHz and secondary peaks around 6 mHz.

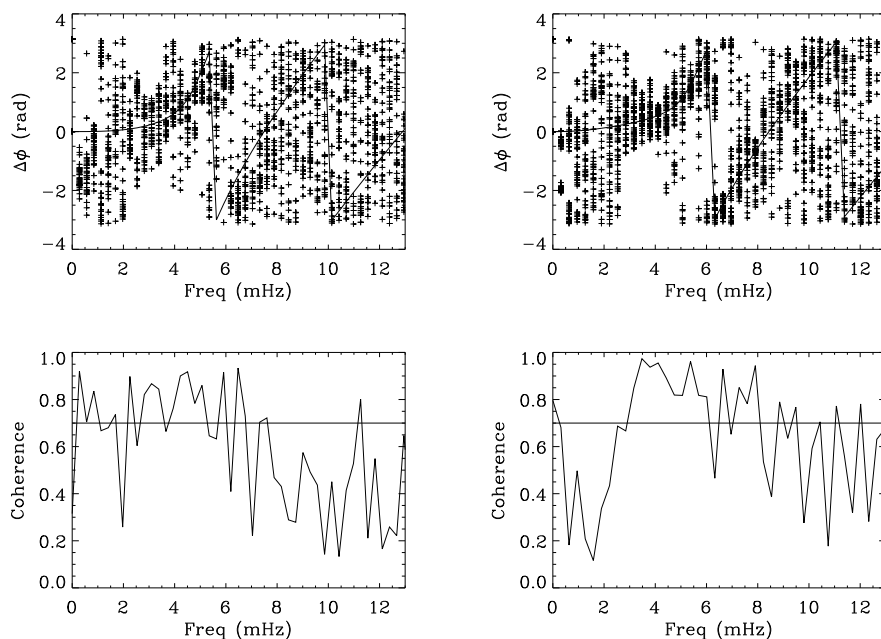


Fig. 6.— **Above:** Phase spectra for all the points in the umbra of sunspot #1 (left) and sunspot #2 (right). On the x-axis the frequency (mHz). On the y-axis, the phase difference between the Fourier transform of the chromospheric velocity oscillation and the photospheric velocity oscillation (radians). The solid line represents the best fit from the theoretical model. **Below:** Coherence spectra for both cases. It gives information about the validity of the phase spectra. Horizontal line sets the confidence limit (coherence greater than 0.7) above which, we can believe the information given by the phase spectrum.

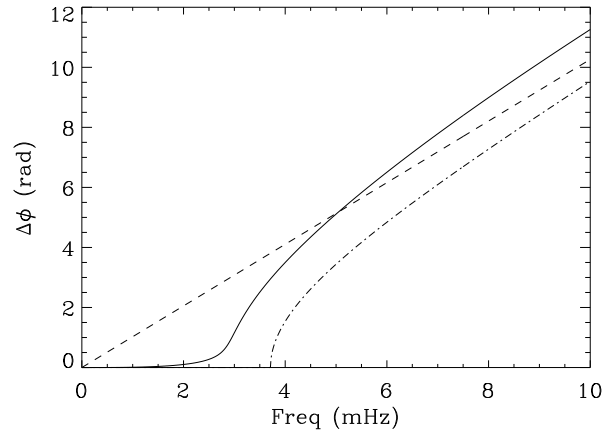


Fig. 7.— **Dashed:** Phase spectrum for linear wave propagation in an isothermal non stratified atmosphere. **Dot-dashed:** the same in a stratified atmosphere (including gravity). **Solid:** The same as the dot-dashed case, but allowing for radiative losses with a Newton’s cooling law ($\tau_R = 15$ s). The same values are applied to the common parameters in the three cases ($T = 9000$ K, $\Delta z = 1600$ km, $g = 274$ m s $^{-2}$).

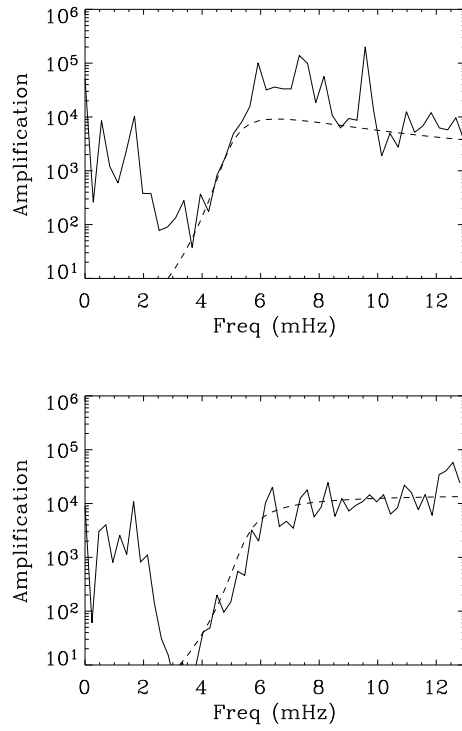


Fig. 8.— **Solid:** Ratio of chromospheric over photospheric power as a function of frequency for data sets 1 (top) and 2 (bottom). **Dashed:** best fit from the model.

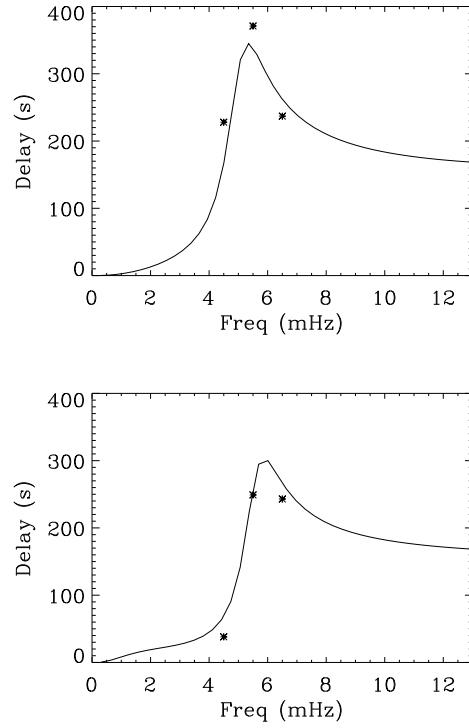


Fig. 9.— Solid line represents the time that it would take for a quasi-monochromatic photospheric perturbation to reach the chromosphere, as a function of frequency, obtained directly from the fits to the phase spectra (sunspot #1 on the top panel and sunspot #2 on the bottom one). Stars represent the measured values of the time delay within 3 narrow filtering bands.

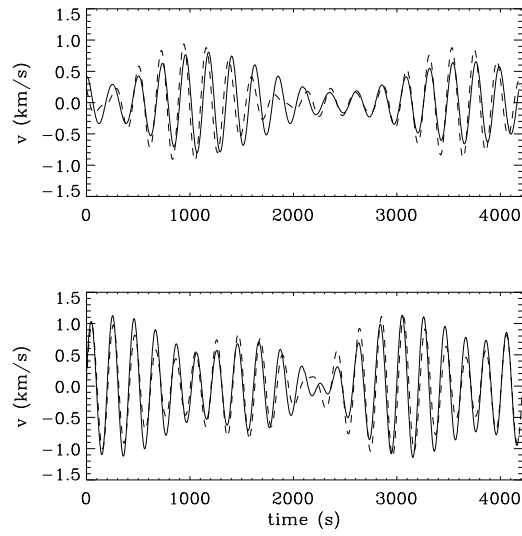


Fig. 10.— **Solid:** Chromospheric velocity signal filtered in the 4 to 5 mHz band for two positions (upper and lower panels) inside umbra #2. **Dashed:** Photospheric filtered velocity signal (in the same band) for the corresponding positions inside the umbra. Photospheric velocity has been amplified by a factor of 20 and shifted forward 38 seconds in order to match the chromospheric one.

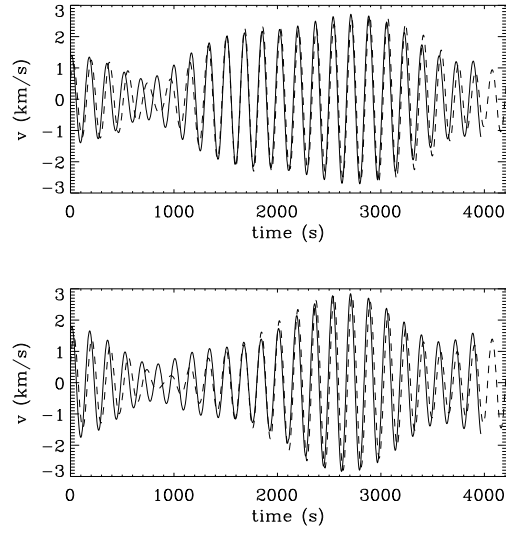


Fig. 11.— Analogous to Fig 10 but in the 5 to 6 mHz range. Photospheric velocity has been amplified by a factor of 80 and shifted forward 242 seconds in order to match the chromospheric one.

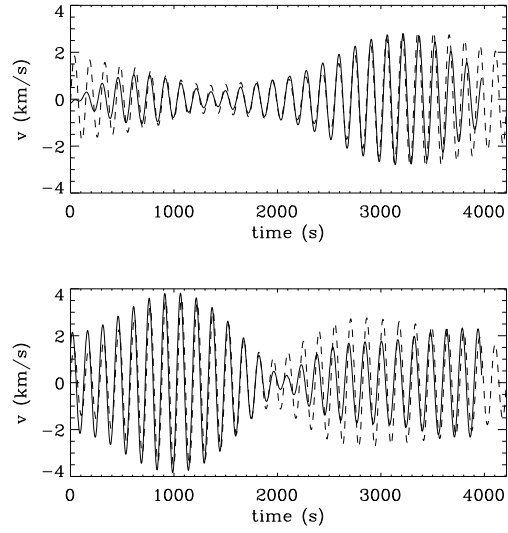


Fig. 12.— Analogous to Fig 10 but in the 6 to 7 mHz range. Photospheric velocity has been amplified by a factor of 80 and shifted forward 248 seconds in order to match the chromospheric one.

Table 1: Details of data sets.

Data set	date	location	umbral size (")	sampling (s)	duration (s)
1	Oct 1st, 2000	11S 2W	16	7.9	3555
2	May 9th, 2001	20N 25W	10	2.1	4200

Table 2: Parameters for phase spectra fits.

Data set	T (K)	Δz (km)	τ_R (s)
1	3400	1000	13
2	4000	1000	55